Light trapping enhancement with combined front metal nanoparticles and back diffraction gratings

Zihuan Xia (夏子奂), Yonggang Wu (吴永刚)*, Renchen Liu (刘仁臣), Pinglin Tang (唐平林), and Zhaoming Liang (梁钊铭)

Institute of Precision Optical Engineering, Tongji University, Shanghai 200092, China

**Corresponding author: ygwu@tongji.edu.cn*

Received November 19, 2012; accepted December 21, 2012; posted online May 29, 2013

In this letter, a design with both metal nanoparticles and back diffraction gratings is put forward for enhancing the efficiency of thin film silicon solar cells. The coupling mechanism between the metal nanoparticles and silicon absorber layer, and that between the incident light and the modes of the silicon absorption layer through the grating layer are both analyzed. The interaction between the front metal nanoparticles and back gratings is analyzed, which substantially increases the light trapping by 58% compared to flat solar cell.

OCIS codes: 350.6050, 050.1950, 250.5403.

doi: 10.3788/COL201311.S10503.

Increasing solar cells efficiency and reducing the cost is the primary objective of research and development on solar cells. Thin film silicon solar cell has efficiently reduced the cost due to the much thinner thickness than crystal silicon solar cells. However the absorption length of silicon material is much larger than the thickness of thin film silicon solar cell, especially in the infrared band. Thus to keep the conversion efficiency, light trapping structure should be introduced to enhance the optical path, such as diffraction grating[1,2], plasmonics[3−5], moth eye antireflection coatings[6,7], etc. Local surface plasmon (LSP) in metal nanoparticles has been widely studied as a promising way to enhance the light absorption for a variety of solar cells[8−11]. Large forward scattering and great near-field enhancement make metal nanoparticles superior to common antireflection coating as the front structure of solar cells[12]. Back diffraction gratings have the potential of achieving better light trapping than Lambertian models in finite spectral range[13]. However, most research groups investigated metal nanoparticles and diffraction grating separately. In this letter, thin film silicon solar cells with combined front core-shell metal nanoparticles and back diffraction grating are investigated. On the one hand, the nanoparticles are intended to reduce the reflection and diffract the incident light into the Si absorber layer. On the other hand, the back grating is intended to diffract back the incident light into the active layer, mainly in the high diffraction orders.

The refractive indexes of c-Si, Ag[15], and ZnO[16] were given. The electromagnetic wave propagation was investigated by finite difference time domain (FDTD) method and rigorous coupled wave analysis (RCWA) using Rsoft software[17]. The quantum efficiency (QE) of a solar cell, $\mathrm{QE}(\lambda)$, is defined by $\mathrm{QE}(\lambda)= P_{\mathrm{abs}}(\lambda)/ P_{\mathrm{in}}(\lambda)$, where $P_{\mathrm{in}}(\lambda)$ and $P_{\mathrm{abs}}(\lambda)$ are the powers of the incident light and absorbed light within the Si solar cell, respectively, at a wavelength λ. All electron-hole pair is assumed to contribute to photocurrent. The short circuit current density J_{sc} is given by $J_{\mathrm{sc}} = e\int \frac{\lambda}{hc}\mathrm{QE}(\lambda)I_{\mathrm{AM1.5}}(\lambda)\mathrm{d}l$, where e is the charge of electron, h is Plank's constant, c is the speed of light in the free space, and $I_{\mathrm{AM1.5}}$ is air mass (AM) 1.5 solar spectrum[18].

Front nanoparticles structure is shown in Fig. 1. 2D arrays of sphere metal cores embedded in ZnO shells are placed on silicon surface. The nanoparticles are characterized by their radius r, period p and are arranged on a hexagonal lattice. The shell thickness d_{ZnO} is 50 nm as a typical antireflection layer for bare silicon without nanoparticles. Reflected diffraction efficiency $R_i(\lambda)$ and transmitted diffraction efficiency $T_i(\lambda)$ at the ZnO/Si interface is recalculated by the weighting function of AM 1.5 solar spectrum as

$$\mathrm{RW}_i = \frac{\sum\limits_{\lambda} R_i(\lambda)I_{\mathrm{AM1.5}}(\lambda)}{N},\ \mathrm{TW}_i = \frac{\sum\limits_{\lambda} T_i(\lambda)I_{\mathrm{AM1.5}}(\lambda)}{N},$$

where i is the diffraction order, and N is the total number of calculated wavelength (400–1 100 nm).

For larger particle sizes, higher order plasmonic resonance modes (multipoles) emerge and the lower order modes are red shifted as a result of dynamic depolarization retardation effects[19]. For Ag nanoparticles in ZnO ambient the surface plasmon resonance wavelength is redshift compare to that in air ambient. Thus the optimum radius in ZnO ambient is smaller than that in air ambient (typically around 100 nm). The size of radius around 50 nm and period of 450 nm is an appropriate choice, as weighted total reflection and transmission of front metal nanoparticles shown in Fig. 2. For r=50 nm, p=450 nm nanoparticles, transmission enhancement can be seen above 700-nm wavelength compare to a typical 50-nm ZnO antireflection coating (dash line) in Fig. 3. The reduction of transmission below 700 nm is ascribed to the absorption of Ag while the reflection slightly increased.

Figure 4 shows the schematic of the back diffraction grating. A ZnO layer is placed between back electrode silver layer and silicon absorber layer as a barrier layer to prevent silicon from metallic impurity. The thickness of ZnO layer, $d_{\mathrm{ZnO,2}}$ is 80 nm. The height and period of back diffraction grating is $h2$ and $p2$, respectively.

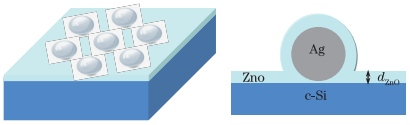

Fig. 1. Schematic of front metal nanoparticles.

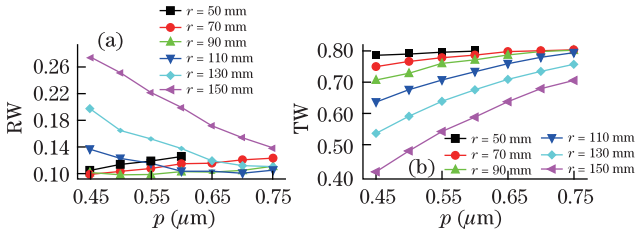

Fig. 2. (Color online) Weighted total (a) reflection and (b) transmission of front metal nanoparticles.

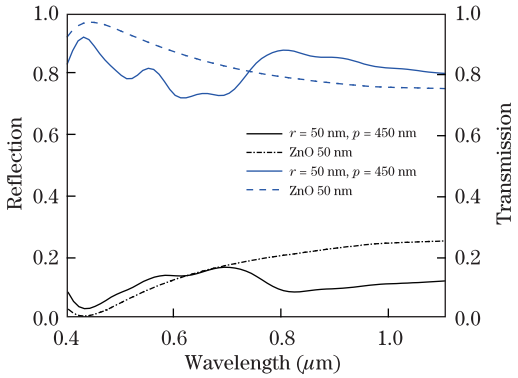

Fig. 3. (Color online) Reflection and transmission of nanoparticles (r=50 nm, p=450 nm) and 50-nm ZnO antireflection coating on silicon substrate.

The grating shape is sinusoidal as a common structure of photolithography. Wavelength considered here is from 500 to 1 100 nm, as the incident light in shorter wavelength is mostly absorbed by the silicon absorber layer.

In order to increase the cell efficiency, the reflected light should be diffracted to higher orders than the 0th order, so the optical path length in silicon absorber layer becomes longer. For grating height larger than 0.2 μm and grating period larger than 0.8 μm, the reflection wave is mainly diffracted in higher diffraction orders and the specular reflection has a minimal value as shown in Fig. 5. For an optimum back grating structure, height and period is chosen as $h2$=0.2 μm, $p2$=0.9 μm. The diffuse reflection is shown in Fig. 6.

So far, the front nanoparticles and the back diffraction gratings had been introduced and optimized separately to select their geometrical parameters. Front nanoparticles and back diffraction gratings were combined from the design rules previously derived. For nanoparticles r=50 nm, p=450 nm and for back grating $h2$=0.2 μm, $p2$=0.9 μm. J_{sc} increased as one could expect with the increase of silicon absorber layer as shown in Fig. 7. However, the increase is nonlinear as it mostly depends on the modes excited by the nanoparticles and back diffraction grating.

For a 300-nm silicon absorber layer, absorption spectra of Ag particle with flat back reflector (red circle) and Ag particle with 2D grating (green up triangle) are depicted in Fig. 8. Ag particle coated 50-nm ZnO on silicon (black square) and 50-nm ZnO antireflection coating with flat back reflector (blue down triangle) are also depicted for reference. Compared to Ag particle with flat back reflector, the higher Si absorption of ZnO coating with flat back reflector in short wavelength (below 500 nm) is ascribed to the lower reflection as shown previously in Fig. 3. And the absorption in Ag particle caused by plasmonic resonance decreased the absorption in Si in short wavelength. However Ag particle excited extra resonance mode at longer wavelength which greatly enhanced absorption in silicon absorber.

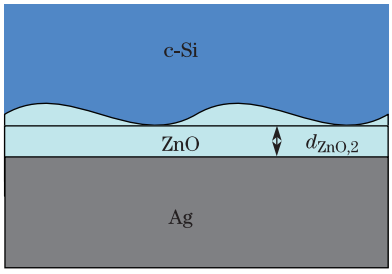

Fig. 4. Schematic of the back diffraction grating.

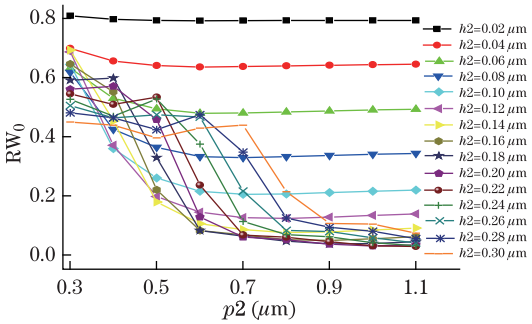

Fig. 5. (Color online) 0th weighted reflection of back grating.

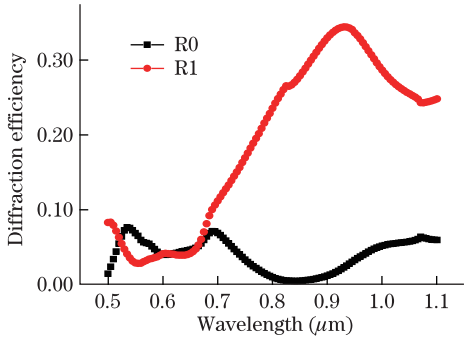

Fig. 6. (Color online) Diffuse reflection of back grating ($h2$=0.2 μm, $p2$=0.9 μm).

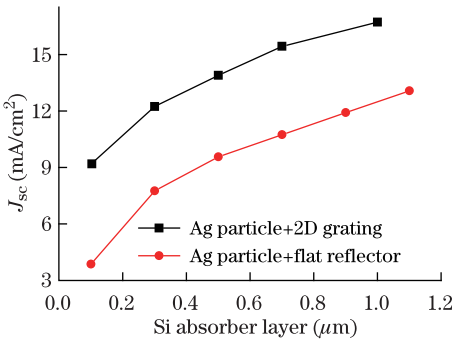

Fig. 7. Short circuit current density versus silicon thickness.

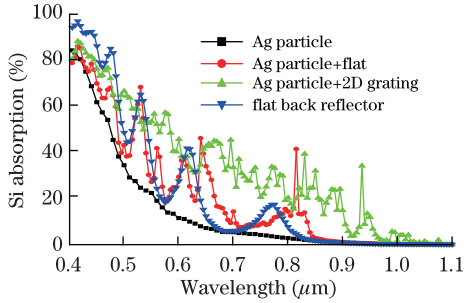

Fig. 8. Absorption spectra of compound structures.

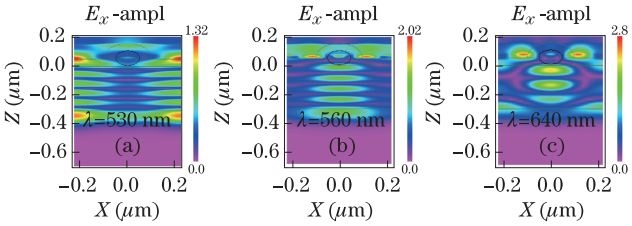

Fig. 9. (Color online) E_x field maps of Ag particle with flat back reflector at (a) λ=530, (b) 560, and (c) 640 nm.

The resonance modes in 530 and 610 nm of Ag particle with flat back reflector (red circle) are ascribed to the Fabry-Perot (FP) resonance which can be seen from the overlapping curve of flat back reflector (blue down triangle). The extra resonance modes excited in 560 and 640 nm of Ag particle with flat back reflector are ascribed to the particle forward scattering as shown in Fig. 9. The electric field distribution at λ=560 nm indicated that most of the absorption took place in the Si absorber layer directly underneath the Ag particles, while at λ=530 nm underneath the ZnO layer without Ag particle. The resonance mode at 530 nm is the FP resonance between ZnO layer and back reflector. The similarity between the electric field distribution at λ=530 and 560 nm indicated that the resonance mode at 560 nm was the FP resonance between the particle and back reflector.

The mixture of FP resonance and particle scattering resulted in a broad peak of absorption from 750 to 850 nm. The electric field distribution at λ=795, 815, and 830 nm were shown in Fig. 10. The large electric field enhancement in most silicon region at λ=815 nm (Fig. 10(b)) implied the sharp peak of the red circle curve in Fig. 8.

Broadband light absorption enhancement was obtained from the nanoparticles and back diffraction grating compound structure (green up triangle in Fig. 8). The enhancement in long wavelength was attributed to the back diffraction grating. The nanopartilce had little effect on the light absorption as the electric field distribution remained the same with or without Ag particle (Figs. 11(a) and (b)). Thus the efficient light trapping by back diffraction grating retained. In visible region the difference of electric field distribution between Figs. 10(c) and (d) indicated that both nanoparticles and gratings had contribution to light absorption. Fortunately the interaction between nanoparticles and gratings led to absorption enhancement in most range of wavelength compared to nanoparticles and flat reflector (Fig. 8) for different thicknesses of Si absorber layer (Fig. 7).

In conclusion, front metal nanoparticles and back diffraction grating are introduced and optimized separately to select their geometrical parameters. The silicon absorber layer is then sandwiched between the nanoparticles arrays which have low reflection and back diffraction grating which reflects incident light mainly into high diffraction orders. FP resonance like modes are excited between nanoparticles and back reflector, which increase the light absorption in solar cell. Light trapping feature of back diffraction grating keeps unchanged for the case with or without nanoparticles in the infrared band. The interaction between nanoparticles and back diffraction grating shows a broadband light absorption enhancement in thin film silicon solar cells. The short circuit current of combined front nanoparticles and back diffraction grating is enhanced by 58% compared to flat back reflector without nanoparticles for a 300-nm silicon absorber layer.

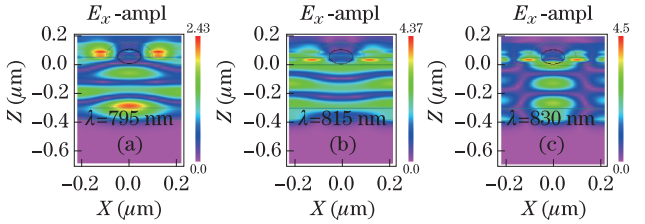

Fig. 10. (Color online) E_x field maps of Ag particle with flat back reflector at (a) λ=795, (b) 815, and (c) 830 nm.

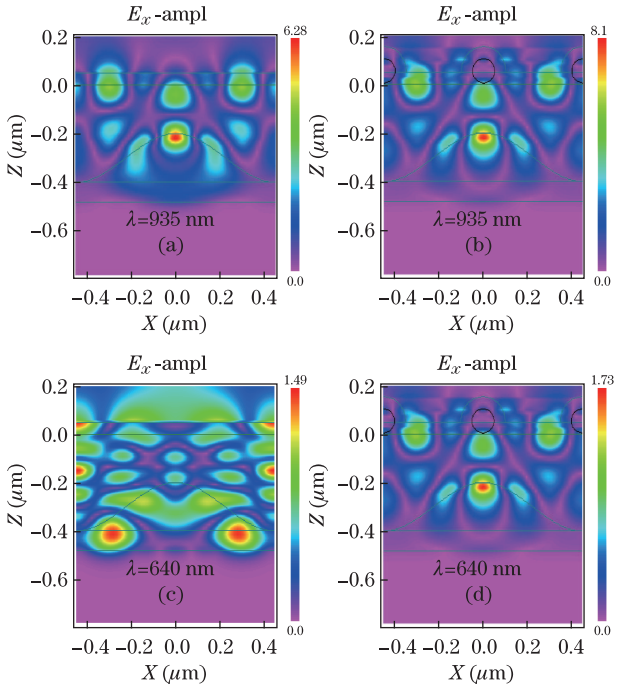

Fig. 11. (Color online) E_x field maps of back diffraction grating at λ=935 nm (a) without and (b) with Ag particle; at λ=640 nm, (c) without and (d) with Ag particle.

This work was supported by the National Natural Science Foundation of China (No. 60977028) and the Key Project Foundation of Shanghai (No. 09JC1413800).

References

1. M. Wellenzohn and R. Hainberger, Opt. Express **20,** A20 (2012).
2. D. Madzharov, R. Dewan, and D. Knipp, Opt. Express **19,** A95 (2011).
3. F. J. Beck, A. Polman, and K. R. Catchpole, J. Appl. Phys. **105,** 114310 (2009).
4. S. Pillai and M. A. Green, Sol. Energ. Mater. Sol. Cell. **94,** 1481 (2010).
5. Z. Sun, X. Zuo, and Y. Yang, Opt. Lett. **37,** 641 (2012).
6. S. A. Boden and D. M. Bagnall, Progress in Photovoltaics: Research and Applications **18,** 195 (2010).
7. N. Yamada, O. N. Kim, T. Tokimitsu, Y. Nakai, and H. Masuda, Progress in Photovoltaics: Research and Applications **19,** 134 (2011).
8. K. R. Catchpole and A. Polman, Opt. Express **16,** 21793 (2008).
9. K. Nakayama, K. Tanabe, and H. A. Atwater, Appl. Phys. Lett. **93,** 121904 (2008).
10. S. D. Standridge, G. C. Schatz, and J. T. Hupp, J. Am. Chem. Soc. **131,** 8407 (2009).
11. S. Pillai, K. R. Catchpole, T. Trupke, and M. A. Green, J. Appl. Phys. **101,** 093105 (2007).
12. P. Spinelli, M. Hebbink, R. de Waele, L. Black, F. Lenzmann, and A. Polman, Nano Lett. **11,** 1760 (2011).
13. X. Sheng, S. G. Johnson, J. Michel, and L. C. Kimerling, Opt. Express **19,** A841 (2011).
14. E. D. Palik, *Handbook of Optical Constants of Solids* (Academic Press, Waltham, 1985).
15. P. B. Johnson and R. W. Christy, Phys. Rev. B **6,** 4370 (1972).
16. "http://refractiveindex.info."
17. "www.rsoftdesign.com/."
18. "http://rredc.nrel.gov/solar/spectra/am1.5/."
19. I. Diukman and M. Orenstein, Sol. Energ. Mater. Sol. Cell. **95,** 2628 (2011).